J Fluoresc (2012) 22:1395–1406
DOI 10.1007/s10895-012-1078-5

ORIGINAL PAPER

Crystal Structures, Interactions with Biomacromolecules and Anticancer Activities of Mn(II), Ni(II), Cu(II) Complexes of Demethylcantharate and 2-Aminopyridine

Fan Zhang · Qiu-Yue Lin · Xiao-Liang Zheng · Ling-Ling Zhang · Qiong Yang · Jia-Ying Gu

Received: 5 October 2011 / Accepted: 11 June 2012 / Published online: 26 June 2012

Abstract Three novel transition metal complexes $(Hapy)_2[M(DCA)_2]\cdot 6H_2O$ (M=Mn(II) (**1**), Ni(II) (**2**), Cu(II) (**3**); DCA= demethylcantharate, 7-oxabicyclo[2.2.1]heptane-2,3-dicarboxylate, $C_8H_8O_5$; Hapy=2-aminopyridine acid, $C_5H_7N_2$) were synthesized and characterized by elemental analysis, infrared spectra, thermogravimetric analysis and X-ray diffraction. DNA binding properties of the complexes were investigated by electronic absorption spectra, fluorescence spectra and viscosity measurements. Results indicated the complexes could bind to DNA through partial intercalation mode with binding constants $K_b/(L\cdot mol^{-1})$ of 1.91×10^4 (**1**), 5.13×10^4 (**2**) and 1.12×10^5 (**3**) at 298 K. Meanwhile, the interactions of the complexes with BSA were also studied by fluorescence spectra. The results suggested that the complexes could quench the fluorescence of BSA through static quenching with the binding constants $K_A/(L\cdot mol^{-1})$ of 1.44×10^6 (**1**), 1.14×10^7 (**2**) and 2.98×10^4 (**3**). And the main contribution was tryptophan residues of BSA. The antiproliferative activity test revealed that complexes showed more intense inhibition ratios against human hepatoma cells lines and human gastric cancer cells lines in vitro. Copper(II) complex (**3**) possesses the strongest inhibition ratio against human hepatoma cells.

F. Zhang · Q.-Y. Lin (✉)
Zhejiang Key Laboratory for Reactive Chemistry on Solid Surfaces, Zhejiang Normal University,
Jinhua, Zhejiang 321004, People's Republic of China
e-mail: sky51@zjnu.cn

F. Zhang · Q.-Y. Lin · L.-L. Zhang · Q. Yang · J.-Y. Gu
College of Chemical and Life Science, Zhejiang Normal University,
Jinhua, Zhejiang 321004, People's Republic of China

X.-L. Zheng
Institute of Materia Medica of Zhejiang Academy of Medical Sciences,
Hangzhou, Zhejiang 310013, People's Republic of China

Keywords Demethylcantharate · 2-aminopyridine · Mn(II) complex · Ni(II) complex · Cu(II) complex · Interaction with biomacromolecules

Introduction

Cantharidin showed unique efficacy for the treatment of hepatoma and oesophageal carcinoma [1, 2]. Demethylcantharidin (NCTD, 7-oxabicyclo[2,2,1] heptane-2,3-dicarboxylc acid anhydride), the derivative of cantharidin, has been used clinically [3]. It not only has strong anti-tumor activity, but also reduced toxicity greatly [4]. Na_2(DCA) (DCA = demethylcantharate, 7-oxabicyclo[2.2.1]heptane-2,3 -dicarboxylate) could inhibit protein serine/threonine phosphatases (PP1, PP2A and PP2B) [5]. The complexes of demethylcantharate have been widely reported, and they possess strong anticancer activities [3, 6]. Meanwhile, some metal complexes containing demethylcantharate and heterocyclic compounds have been reported, which show strong DNA-binding abilities [7, 8] and intense anticancer activities [9–11]. Pyridine is an important class of N-containing heterocycles. The complexes containing pyridine ring have been reported for their bioactivities, such as DNA binding property and antibacterial activity [12, 13]. Meanwhile, ionic compounds possess the advantages of the better water-solubility, easily channel through cell membranes and so on.

According to the literature [14], the platinum complexes containing DCA likely possess dual anti-cancer mechanism: inhibition of PP2A and interaction with DNA, which promotes the anticancer activities of complexes. So design and synthesize the drugs, which could simultaneously interact with various biomacromolecules (such as DNA and protein) strongly, have the vital significance.

Thus, we synthesized three novel transition metal complexes $(Hapy)_2[M(DCA)_2]\cdot 6H_2O$ (M=Mn(II) (**1**); Ni(II) (**2**); Cu(II)

(**3**)) by metal acetate, NCTD and 2-aminopyridine (apy). The interactions of the complexes with DNA were investigated by electronic absorption spectra, fluorescence spectra and viscosity measurements. And the interaction of the complexes with BSA was studied by fluorescence spectra. In addition, the antiproliferative activities of the complexes against human hepatoma cells (SMMC-7721) and human gastric cancer cells (MGC80-3) were tested in vitro. The probable antiproliferative mechanism was discussed preliminarily.

Experimental Sections

Materials and Instruments

All reagents and chemicals were obtained from commercial sources. Demethylcantharidin (NCTD, $C_8H_8O_4$) was obtained from Nanjing Zelang Medical Technology Co. Ltd.; Ethidium bromide (EB) was obtained from Fluka Co.; 2-aminopyridine (apy, $C_5H_6N_2$) and DNA were obtained from Sinopharm Chemical Reagent Co. Ltd.; DNA (ρ=200 μg·mL^{-1}, c=3.72×10^{-4} mol·L^{-1}), which A_{260}/A_{280}=1.8 – 2.0, was prepared by 50 mmol·L^{-1} NaCl; Bovine Serum Albumin (BSA) was purchased from Beijing BioDee BioTech Co. Ltd. and was stored at 277 K; BSA (ρ=500 μg·mL^{-1}, c=7.47×10^{-6} mol·L^{-1}) was prepared by 5 mmol·L^{-1} NaCl; Human hepatoma cells (SMMC-7721) and human gastric cancer cells (MGC80-3) were purchased from Shanghai Institute of Cell Bank. Other chemical reagents in analytical reagent grade were used without further purification.

Elemental analyses of C, H and N were carried out in Vario EL III elemental analyzer. Infrared spectra were measured using the KBr disc method by NEXUS-670 FT-IR spectrometer in the spectral range 4,000–400 cm^{-1}. The thermogravimetric analyses were monitored on TGA/SDTA851^e thermo gravimetric analyzer. Diffraction intensities of the complexes were collected at 293 K on Bruker SMART APEX II CCD difffractometer. Electronic absorption spectra were recorded on UV-2501 PC spectrophotometer. Fluorescence emission spectra were obtained by Perkin-Elmer LS-55 spectrofluorometer. Viscosity experiments were carried on Ubbelodhe viscometer.

Synthesis of the Complexes

The solution of $M(Ac)_2{\cdot}6H_2O$ (0.5 mmol, M=Mn(II), Ni(II) and Cu(II)) and 2-aminopyridine (0.5 mmol) were stirred at the room temperature for 2 h. The solution of NCTD (0.5 mmol) was added dropwise into the mixed solution. The pH of the solution was adjusted to 6.5 using dilute NaOH solution. The solution was then filtered after two hours. Two weeks later, crystals with suitable size for single-crystal X-ray diffraction were obtained.

Anal. Calc (%). for $C_{26}H_{42}N_4O_6Mn$ (**1**): C, 43.24; H, 5.82; N, 7.76. Found (%): C, 43.47; H, 5.84; N, 7.60. Anal. Calc (%). for $C_{26}H_{42}N_4O_6Ni$ (**2**): C, 43.01; H, 5.79; N, 7.72. Found (%): C, 42.91; H, 5.87; N, 7.23. Anal. Calc (%). for $C_{26}H_{42}N_4O_6Cu$ (**3**): C, 42.73; H, 5.75; N, 7.67. Found (%): C, 43.19; H, 6.04; N, 7.79.

The values of molar conductance of complexes **1**–**3** are in the range of 142–158 s·cm^2·mol^{-1} in 10^{-3} mol·L^{-1} DMF at 20 °C, which suggest that the complexes are 2:1 type electrolytes [15].

DNA Binding

Electronic Absorption Spectra

Electronic absorption spectra experiments were carried out at 25 °C by fixing the concentrations of the complexes (2.50×10^{-5} mol·L^{-1}) or 2-aminopyridine (5.00×10^{-5} mol·L^{-1}). The amounts of DNA were increasing over concentration range of 0 to 2.50×10^{-5} mol·L^{-1}. Absorption spectra measurements were carried out at 200 nm - 400 nm in Tris–HCl buffer (pH=7.4), and DNA solution was used as reference.

Fluorescence Spectra

Fluorescence quenching experiments were carried out by adding complexes solutions (0–2.50×10^{-4} mol·L^{-1}) to samples solutions containing 5.00×10^{-6} mol·L^{-1} EB and 7.44×10^{-5} mol·L^{-1} DNA. The mixture were diluted by Tris–HCl buffer solution (pH=7.4). Fluorescence was recorded at excitation wavelength (λ_{ex}) at 252 nm and emission wavelength (λ_{em}) between 500 nm and 700 nm.

Viscosity Measurements

Viscosity measurements were carried out at 25 °C. Compounds were added into DNA solution (3.72×10^{-4} mol·L^{-1}), and the concentration of the compounds were controlled within the range of 0–3.33×10^{-6} mol·L^{-1}. The relative viscosities η were calculated using equation [16]: $\eta=(t - t_0)/t_0$, where t_0 and t represent the flow time of DNA solution through the capillary in the absence and presence of complex.

Interaction with BSA

Fluorescence Spectra

Different amount of complexes solutions (0–4.00×10^{-8} mol·L^{-1}) were added to the samples containing 4.98×10^{-7} mol·L^{-1} BSA and Tris–HCl buffer (pH=7.4). Fluorescence spectra were obtained by recording the emission spectra (260 nm – 500 nm) corresponding to excitation wavelength at 260 nm.

Synchronous Fluorescence Spectra

Synchronous fluorescence spectra were scanned at the same conditions as in Section 2.4.1. The spectra were measured at two different $\Delta\lambda$ ($\Delta\lambda=\lambda_{em}-\lambda_{ex}$) values, which were 15 nm and 60 nm.

Antiproliferative Activity Evaluation

The antiproliferative activities of Na_2DCA and the complexes were evaluated by human hepatoma cells (SMMC-7721) and human gastric cancer cells (MGC80-3). The antiproliferative activities were measured by the MTT assay. The compounds were dissolved in DMSO as 100 mmol·L^{-1} stock solutions and diluted with culture medium before using. Cells were seeded for 24 h, and the complexes or $Na_2(DCA)$ were added and incubated for 72 h. Then MTT (100 μL, 1 mg·mL^{-1}, dissolved in culture medium) was added into each well and incubated for 4 h (37 °C). The inhibition rate was calculated. The errors quoted were standard deviations, in which three replicates were used in the calculation [17].

Crystal Structure Determination

Single crystals, sized 0.204 mm×0.282 mm×0.378 mm (**1**), 0.073 mm×0.236 mm×0.372 mm (**2**) and 0.200 mm×0.293 mm×0.331 mm (**3**), were analyzed by X-ray diffraction. Their structures were solved by direct methods and refined by full-matrix least-squares techniques using the SHELXL-97 program package [18, 19]. All non-hydrogen atoms were refined anisotropically. Besides the hydrogen atoms on oxygen atoms were located from the difference Fourier maps, the other hydrogen atoms were generated geometrically. Crystal data and experimental details for structural analyses are listed in Table 1.

Results and Discussion

Characterization and Crystal Structures of the Complexes

Infrared Spectra (IR)

Three complexes have similar infrared spectra, which suggest that they have similar structures. According to the

Table 1 Crystal Data and Structure Refinement Details for Complexes **1** - **3**

Complex	**1**	**2**	**3**
Chemical formula	$MnC_{26}H_{42}N_4O_{16}$	$NiC_{26}H_{42}N_4O_{16}$	$CuC_{26}H_{42}N_4O_{16}$
Formula weight	721.58	725.33	730.19
Crystal system	Triclinic	Triclinic	Triclinic
Space group	$P\bar{1}$	$P\bar{1}$	$P\bar{1}$
a (Å)	6.59190 (10)	6.6060 (2)	6.6438 (6)
b (Å)	10.24810 (10)	10.1215 (2)	10.1670 (10)
c (Å)	11.9367 (2)	11.9532 (3)	11.8994 (11)
α (°)	92.2450 (10)	92.9490 (10)	93.142 (4)
β (°)	90.5070 (10)	90.215 (2)	90.277 (4)
γ (°)	98.2430 (10)	99.5890 (10)	98.657 (4)
Volume (Å^3)	797.35 (2)	786.95 (3)	793.35 (13)
Z	1	1	1
Shape	block	block	block
Color	colorless	green	green
D_c (g/cm^{-3})	1.503	1.531	1.528
θ Rang for data collection (°)	1.71 to 25.00	1.71 to 25.00	1.71 to 25.00
Reflections collected/Unique	8828/2573	8901/2543	10840/2783
R(int)	0.0396	0.0320	0.0185
Absorption coefficient (mm^{-1})	0.495	0.698	0.769
F (000)	379	382	383
R/wR [$I>2\sigma(I)$]	0.0622/0.1776	0.0346/0.0865	0.0418/0.1223
Restraints/parameters	15/214	9/214	3/214
Goodness-of-fit on F^2	1.246	0.930	1.034
Largest diff. Peak and hole (e·Å^{-3})	0.613, −1.014	0.376, −0.547	0.692, −0.671

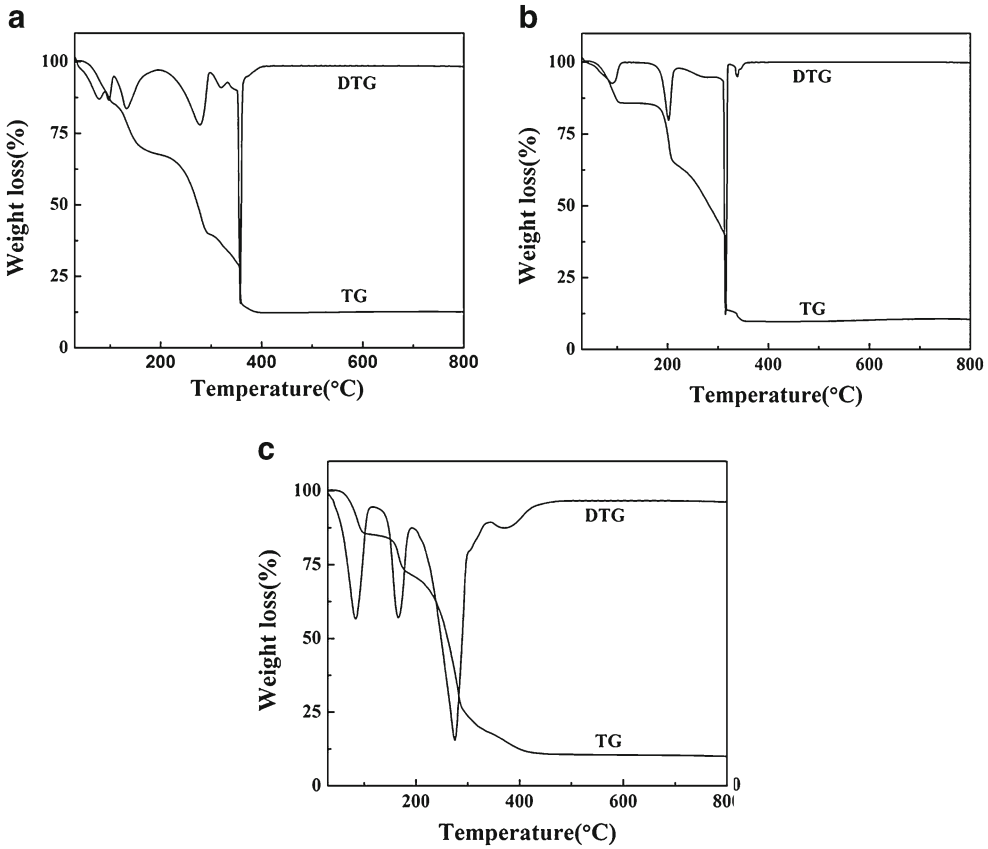

Fig. 1 The TG-DTG curves of complexes. **a** complex **1**; **b** complex **2**; **c** complex **3**

comparison of the IR spectra of the complexes with the free ligands (Na_2(DCA) and 2-aminopyridine), characteristic absorption peaks in IR spectra were assigned. The complexes have characteristic bands of asymmetric stretching vibration (ν_{as} (COO^-)) at 1688 (**1**), 1689 (**2**) and 1685 cm^{-1} (**3**) and symmetric stretching vibration (ν_s (COO^-)) at 1413 (**1**), 1414 (**2**) and 1413 cm^{-1} (**3**). The $\Delta\nu=\nu_{as}$ (COO^-) - ν_s (COO^-) are greater than the value of Na_2(DCA) (180 cm^{-1}), which indicates that the carboxylate groups are monodentate coordination to the metal ion [20]. The characteristic band of stretching vibration for ν (C-O-C) is 1257 cm^{-1}, while the stretching vibration peaks of ether skeleton are at 1059 and 995 cm^{-1}. Compared to the ligand, peaks of ν (C-O-C) in complexes shift to 1262 cm^{-1} –1266 cm^{-1}; 1031 cm^{-1} – 1032 cm^{-1} and

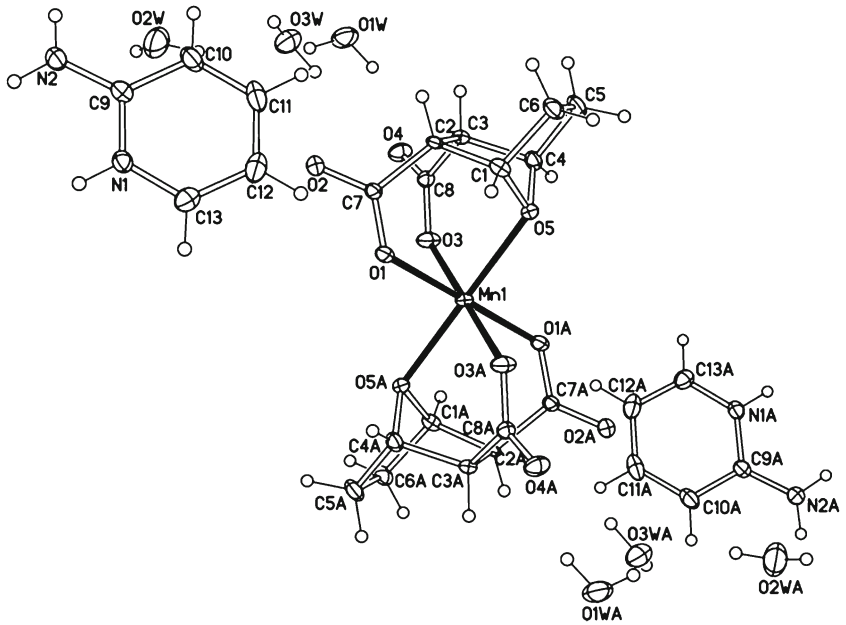

Fig. 2 Molecular structure of complex **1**

984 cm^{-1} – 986 cm^{-1}, which suggest that cyclic ether oxygen involves in this coordination [8]. However, there is no obvious characteristic band shift in 2-aminopyridine, which indicate that 2-aminopyridine don't take part in the coordination. Meanwhile, there are strong bands at wavelength around 3200 cm^{-1} of the complexes **1**–**3**, which suggests that the structures of the complexes contain crystal water.

Thermogravimetric Analysis (TGA)

The thermogravimetric analysis (TGA) experiment was performed under air atmosphere with heating rate of 10 °C·min^{-1}, and the temperature was controlled in 30 °C – 800 °C. The TG-DTG curves of complexes are shown in Fig. 1(a: (**1**); b: (**2**); c: (**3**)). Three complexes had similar thermal behaviors. A three-step weight losing process was involved in this experiment. Here, complex **1** (Fig. 1 (a)) was taken as an example to analyze the thermolysis process. According to Fig. 1 (a), the first step weight loss (14.26 %), which corresponds to the departure of the six crystal water (15.05 % theoretical), occurred at the range of 53 °C - 102 °C. The second weight loss (25.62 %), which corresponded to the departure of two 2-aminopyridine acids (26.34 % theoretical), was occurred in the temperature range of 103 °C – 251 °C. The complex gave an acuity weight loss peak at temperature around 252 °C – 398 °C, which corresponded to the weigh loss of 47.65 % (48.78 % theoretical). It also indicated the thermal decomposition of two DCA. At temperature above 398 °C, no further weight loss would occur. The sample residue was MnO, which weigh 10.70 % of the initial mass (9.83 % theoretical).

At temperature above 355 °C (**2**) and 443 °C (**3**), the weight of complexes were invariant. The residues were metallic oxide of central ions NiO (**2**) and CuO (**3**). These results agree with the composition of the complexes, which were determined by elemental analyses and X-ray diffraction.

Structural Description of Complexes

The X-ray structural analysis shows that the types and the positions of atoms in the complexes are quite similar with each other, besides the metal ions. They have the same space group ($P\bar{1}$) and similar unit cell dimensions. Since extensive hydrogen-binding interactions exist in complexes **1**–**3**, complex **1** is taken as an example for structural analyze.

Molecular structure of the complex $(Hapy)_2[Mn(DCA)_2]\cdot 6H_2O$ (**1**) is shown in Fig. 2. Selected bond distances and angles are listed in Table 2. Complex **1** is consisted by cation part and anion part (Fig. 2). Each Mn(II) ion connected to two DCA ions, which formed anion part. And the cation part was formed by two 2-aminopyridine acids. Mn(II) ion was six-coordinated by four carboxylate oxygen atoms O1, O3, O1A and O3A in four different carboxylate groups and two bridge oxygen atoms O5 and O5A from two demethylcantharates, which formed octahedral structure. Due to the binding of the bridge oxygen atoms O5 and O5A with Mn (II), four six-membered rings (Mn1-O1-C7-C2-C1-O5), (Mn1-O3-C8-C3-C4-O5), (Mn1-O1A-C7A-C2A-C1A-O5A) and (Mn1-O3A-C8A-C3A-C4A-O5A) were created. Two seven-membered rings (Mn1-O1-C7-C2-C3-C8-O3) and (Mn1-O1A-C7A-C2A-C3A-C8A-O3A) were formed because of the coordination of carboxylate oxygen atoms O1, O1A, O3 and O3A, which could have stabilized the anion part of complex **1**.

Selected bond distances and angles of other complexes are listed in Table 3 (**2**) and Table 4 (**3**).

Table 2 Selected bond lengths (Å) and angles (°) for complex **1.** Symmetry transformations used to generate equivalent atoms: #1 -x,-y,-z

Bond	(Å)	Bond	(Å)
Mn(1)–O(1)	2.1896(10)	Mn(1)–O(1)#1	2.1896(10)
Mn(1)–O(3)	2.1092(10)	Mn(1)–O(3)#1	2.1092(10)
Mn(1)–O(5)	2.2508(9)	Mn(1)–O(5)#1	2.2508(9)
Angle	(°)	Angle	(°)
O(1)-Mn(1)-O(5)	86.21(3)	O(1)-Mn(1)-O(5)#1	93.79(3)
O(1) -Mn(1)-O(1)#1	180.00(6)	O(1)#1-Mn(1)-O(5)	93.79(3)
O(1)#1-Mn(1)-O(5)#1	86.21(3)	O(3)-Mn(1)-O(1)	85.93(4)
O(3)-Mn(1)-O(1)#1	94.07(4)	O(3)-Mn(1)-O(3)#1	180.00(7)
O(3)#1-Mn(1)-O(1)	94.07(4)	O(3)#1-Mn(1)-O(1)#1	85.93(4)
O(3)-Mn(1)-O(5)	86.62(4)	O(3)-Mn(1)-O(5)#1	93.38(4)
O(3)#1-Mn(1)-O(5)	93.38(4)	O(3)#1-Mn(1)-O(5)#1	86.62(4)
O(5) -Mn(1)-O(5)#1	180.00(5)		

Table 3 Selected bond lengths (Å) and angles (°) for complex **2.** Symmetry transformations used to generate equivalent atoms: #1 -x,-y+1,-z

Bond	(Å)	Bond	(Å)
Ni(1)–O(1)	2.0226(11)	Ni(1)–O(1)#1	2.0226(11)
Ni(1)–O(3)	2.0697(10)	Ni(1)–O(3)#1	2.0697(10)
Ni(1)–O(5)	2.0990(10)	Ni(1)–O(5)#1	2.0990(10)
Angle	(°)	Angle	(°)
O(1)–Ni(1)–O(1)#1	180.00(6)	O(1)–Ni(1)–O(3)	87.42(4)
O(1)#1–Ni(1)–O(3)	92.58(4)	O(1)–Ni(1)–O(3)#1	92.58(4)
O(1)#1–Ni(1)–O(3)#1	87.42(4)	O(3)#1–Ni(1)–O(3)	180.00(6)
O(1)–Ni(1)–O(5)	91.36(4)	O(1)#1–Ni(1)–O(5)	88.64(4)
O(3)–Ni(1)–O(5)	90.74(4)	O(3)#1–Ni(1)–O(5)	89.26(4)
O(1)–Ni(1)–O(5)#1	88.64(4)	O(1)#1–Ni(1)–O(5)#1	91.36(4)
O(3)–Ni(1)–O(5)#1	89.26(4)	O(3)#1–Ni(1)–O(5)#1	90.74(4)
O(5)#1–Ni(1)–O(5)	180.00(5)		

Table 4 Selected bond lengths (Å) and angles (°) for complex **3**. Symmetry transformations used to generate equivalent atoms: #1 -x,-y+1,-z

Bond	(Å)	Bond	(Å)
Cu(1)–O(1)	2.0677(19)	Cu(1)–O(1)#1	2.0677(19)
Cu(1)–O(3)	1.9343(18)	Cu(1)–O(3)#1	1.9343(18)
Cu(1)–O(5)	2.2831(19)	Cu(1)–O(5)#1	2.2831(19)
Angle	(°)	Angle	(°)
O(1)-Cu(1)-O(1)#1	180.00(10)	O(1)-Cu(1)-O(5)	89.08(7)
O(1)-Cu(1)-O(5)#1	90.92(7)	O(1)#1-Cu(1)-O(5)	90.92(7)
O(1)#1-Cu(1)-O(5)#1	89.08(7)	O(3)-Cu(1)-O(1)	88.62(8)
O(3)-Cu(1)-O(5)	89.91(7)	O(3)-Cu(1)-O(1)#1	91.38(8)
O(3)#1-Cu(1)-O(1)	91.38(8)	O(3)-Cu(1)-O(3)#1	180.00(11)
O(3)-Cu(1)-O(5)#1	90.09(7)	O(3)#1-Cu(1)-O(5)	90.09(7)
O(3)#1-Cu(1)-O(1)#1	88.62(8)	O(3)#1-Cu(1)-O(5)#1	89.91(7)
O(5)#1-Cu(1)-O(5)	180.00(8)		

DNA Bingding Studies

Electronic Absorption Spectra

To study the interaction mode and intensity of complexes with DNA, we used titration to test the effect of DNA to the complexes in UV absorption spectra at 298 K. Results are shown in Fig. 3 (a (**1**), b (**2**), c (**3**)). According to the spectra, the complexes have similar absorption peaks. The absorption bands of complexes appear at 229 nm and 285 nm, which are mainly contributed by the ligand 2-aminopyridine. $Na_2(DCA)$ cannot be characterized with UV absorption spectra. The hypochromic effect emerged with increasing the concentration of DNA.

The intrinsic binding constants (K_b) were determined by the equation [21]: $[DNA]/(\varepsilon_A - \varepsilon_F)=[DNA]/(\varepsilon_B - \varepsilon_F)+1/[K_b(\varepsilon_B - \varepsilon_F)]$. In the plots of $[DNA]/(\varepsilon_A - \varepsilon_F)$ versus [DNA], K_b are given by the ratio of the slope to intercept. The binding constants K_b/(L·mol^{-1}) for the complexes were 5.95×10^3 (apy), 1.91×10^4 (**1**), 5.13×10^4 (**2**) and 1.12×10^5 (**3**), respectively. The values suggested that the interaction intensity with DNA of the complexes were stronger than 2-aminopyridine, and complex **3** possesses the strongest interaction. After the complexes being formed, the binding intensity with DNA increased. Compared to some other copper(II) complexes, the K_b of complex **3** is slightly lower than that of copper(II) phenanthroline complex [Cu(acac)(dppz)Cl] (2.16×10^5 L·mol^{-1}) [22] and higher than that of copper(II) aniline complex [$CuL_2(OAc)_2$] (2.88×10^3 L·mol^{-1}) [23]. The comparison shows that the larger the planar rings of aromatic heterocyclic ligands are, or the more the numbers of heteroatom are, more intense the interactions are.

Fluorescence Spectral Studies

To study the mode and intensity of the interaction of complexes with DNA, EB was used as fluorescence probe. The

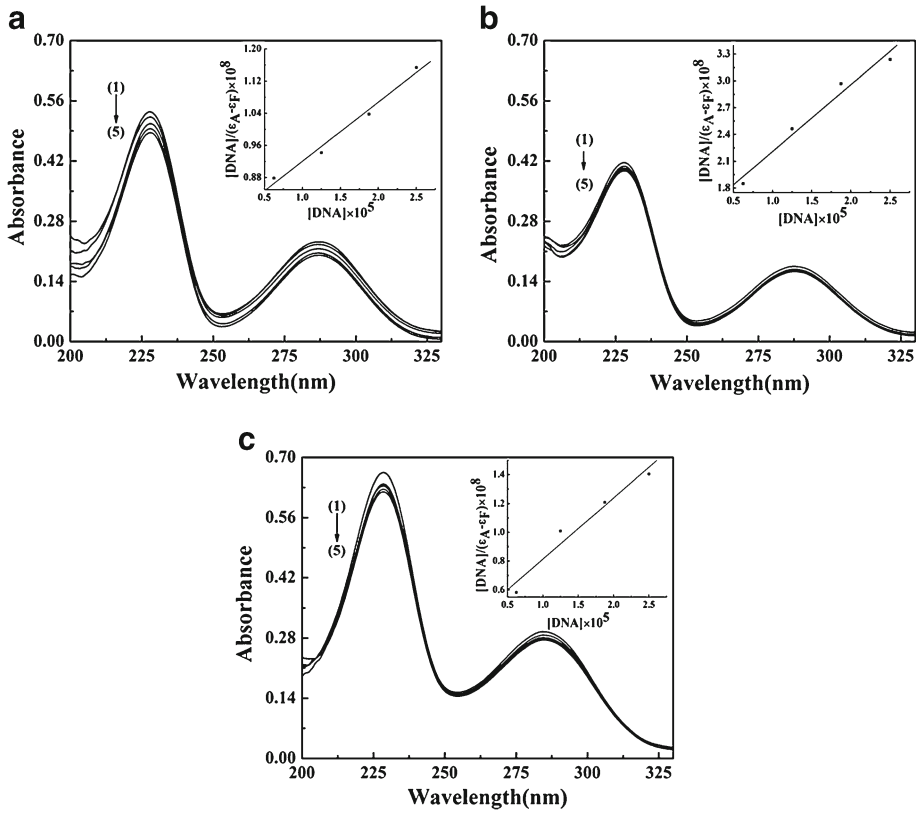

Fig. 3 Absorption spectra of the complexes in the presence of increasing amount of DNA at 298 K. [complex]=2.50×10^{-5} mol·L^{-1}, from (1) to (5): [DNA]$\times10^5$=0, 0.63, 1.25, 1.88 and 2.50 mol·L^{-1}, respectively. **a** complex **1**; **b** complex **2**; **c** complex **3**

complexes quenched the fluorescence of EB-DNA system was studied. Figure 4 shows the emission spectra of EB bounded to DNA with 2-aminopyridine (Fig. 4a) and the complexes (Fig. 4b - d) with similar peak shapes. Figure 4 suggests that, as the concentrations of the compounds increasing, the emission intensity at 589 nm of EB-DNA system decrease in different degrees.

According to the Stern-Volmer equation [24]: $F_0/F=1+K_{sq}$ r, where F_0 and F represent the fluorescence intensities in the absence or presence of complexes, r stands for the concentration ratio of the complexes to DNA. The quenching constant K_{sq} was obtained as the slope of F_0/F versus r linear plot, which were 0.058 (apy), 0.15 (**1**), 0.18 (**2**) and 1.37 (**3**). It indicated that the complexes could release free EB from EB-DNA system. The quenching ratios (F_0/F) of complexes exceed two times of 2-aminopyridine according to Fig. 4, which infers that there is a synergistic effect on quenching the fluorescence of EB-DNA, due to the existence of [M(DCA)$_2$] ion. However, NCTD and Na$_2$(DCA) can not quench the emission intensities of EB-DNA system significantly [25].

Viscosity Measurements

To further investigate the binding mode and binding intensity of the complexes with DNA, the DNA viscosity changing at 25 °C was studied (Fig. 5). The average values of three replicated measurements were used to evaluate the viscosity of the samples. Data were presented as $(\eta/\eta_0)^{1/3}$ versus the ratio of the concentration of compounds to DNA, where η is the viscosity of DNA in the presence of compound and η_0 is the viscosity of DNA alone. The result showed that the relative viscosity of DNA steadily decreased after adding complexes. But there was no obvious viscosity change happened after adding 2-aminopyridine and NCTD, which suggested that the complexes may partially insert into DNA [26]. But free ligands couldn't intercalate DNA significantly. Structurally, the cation pyridine ring can insert into the DNA base pairs. However, viscosity studies show that the effect would only be enhanced when the anion parts of complexes exist. However, the steric hindrance of the complexes is accrescent due to the non-planar of DCA. Thus, the complexes can only partially insert into DNA. And the binding constant K_b (5.93×10^5 L·mol^{-1}) [27] of the classical intercalator ethidium bromide (EB) with DNA was one or two orders of magnitude higher than K_b of complexes **1**–**3**. So the binding mode between the complexes and DNA is partial intercalation.

Meanwhile, the relative viscosity of DNA reduces in different degree, which infers that the binding intensities of the complexes are different with the order of **3**>**2**>**1**. And this order reflects that the effect ability of different central metal ions to the interactions between complexes and DNA is Cu(II) >Ni(II)>Mn(II). The result agrees with the UV-visible absorption spectra and fluorescence spectra.

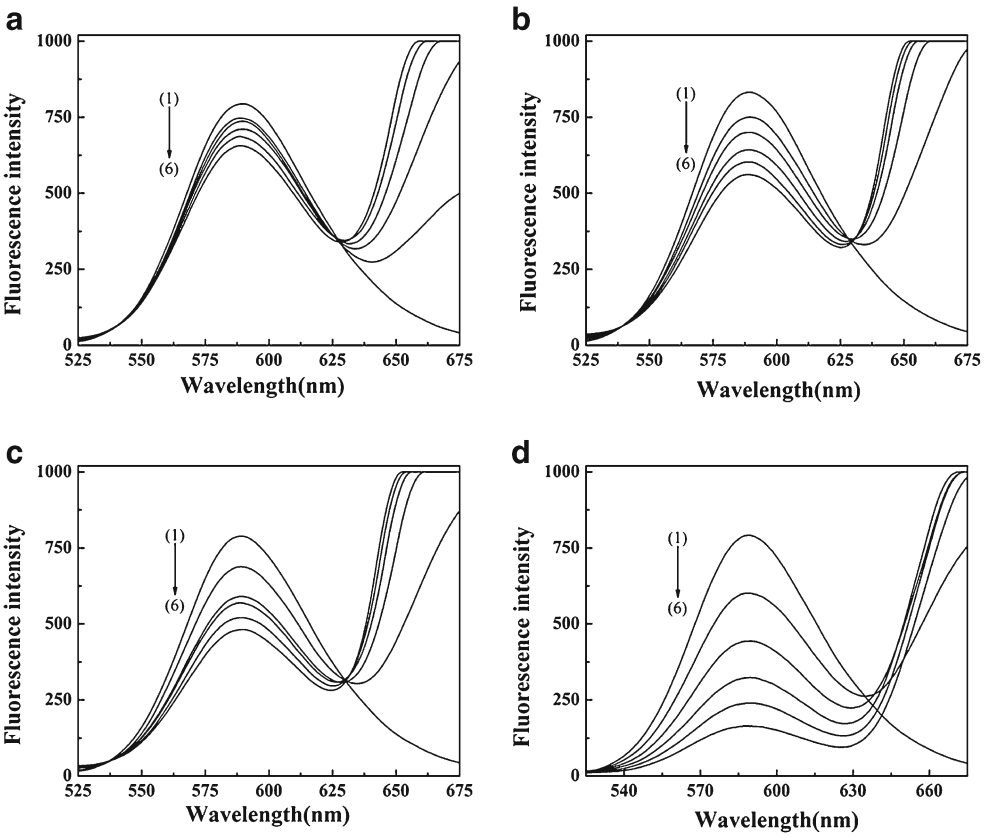

Fig. 4 Fluorescence spectra of EB-DNA in the absence and presence of increasing the amount of compounds (λ_{ex}=252 nm). [EB]=5.00×10^{-6} mol·L^{-1}; [DNA]=7.44×10^{-5} mol·L^{-1}; r=[complex]/[DNA]=0, 0.67, 1.34, 2.02, 2.69 and 3.36, from (1) to (6), respectively. **a** 2-aminopyridine; **b** complex **1**; **c** complex **2**; **d** complex **3**

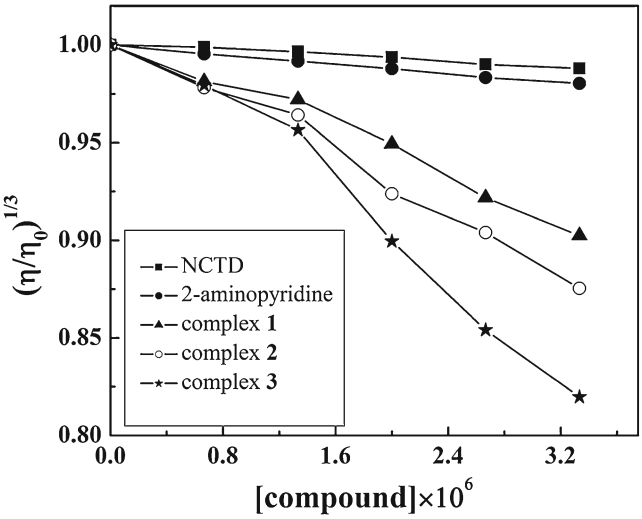

Fig. 5 Effect of increasing amounts of the compounds on the relative viscosity of DNA, at 25 °C. [DNA]=3.72×10^{-4} mol·L^{-1}; [compound]×10^6=0, 0.67, 1.33, 2.00, 2.67 and 3.33 mol·L^{-1}, respectively

Interaction with BSA

Fluorescence Spectra and Quenching Mechanism

The fluorescence quenching of BSA by the complexes are shown in Fig. 6 (a (**1**), b (**2**), c (**3**), d (NCTD)). The results showed that BSA had strong fluorescence emission at 345 nm. The peak intensity decreased with the increasing concentration of complexes, which inferred that strong interactions and energy transfer between complexes and BSA existed [28].

In order to verify the quenching mechanism, the fluorescence quenching was assumed to be dynamic quenching. The quenching rate constants can be calculated by the Stern-Volmer equation[29]: $F_0/F=1+K_q\ \tau_0\ [Q]$, where F_0 and F are the fluorescence intensities of BSA in the absence and presence of the complexes, respectively, τ_0 is approximately 10^{-8} s [30], *[Q]* is the concentration of the complexes. The calculated quenching rate constants K_q/(L·mol^{-1}·s^{-1}) were 6.40×10^{14} (**1**), 1.05×10^{15} (**2**) and 1.05×10^{15} (**3**), respectively. These values are much higher than the maximum possible value for diffusion-limited quenching in water (2×10^{10} L·mol^{-1}·s^{-1}), which suggests that quenching mechanism of complexes to BSA is static quenching [31].

Binding Constants and Binding Sites

Assuming there were n identical and independent binding sites in protein, the binding constant K_A can be calculated using equation [32]: lg $(F_0 - F)/F$=lg K_A+n lg [Q], K_A and n were calculated by linear fitting of a plot of lg $(F_0$-$F)/F$ against lg *[Q]* (Fig. 7). The values of K_A/(L·mol^{-1}) were 2.78×10^4 (NCTD), 1.44×10^6 (**1**), 1.14×10^7 (**2**) and 2.98×

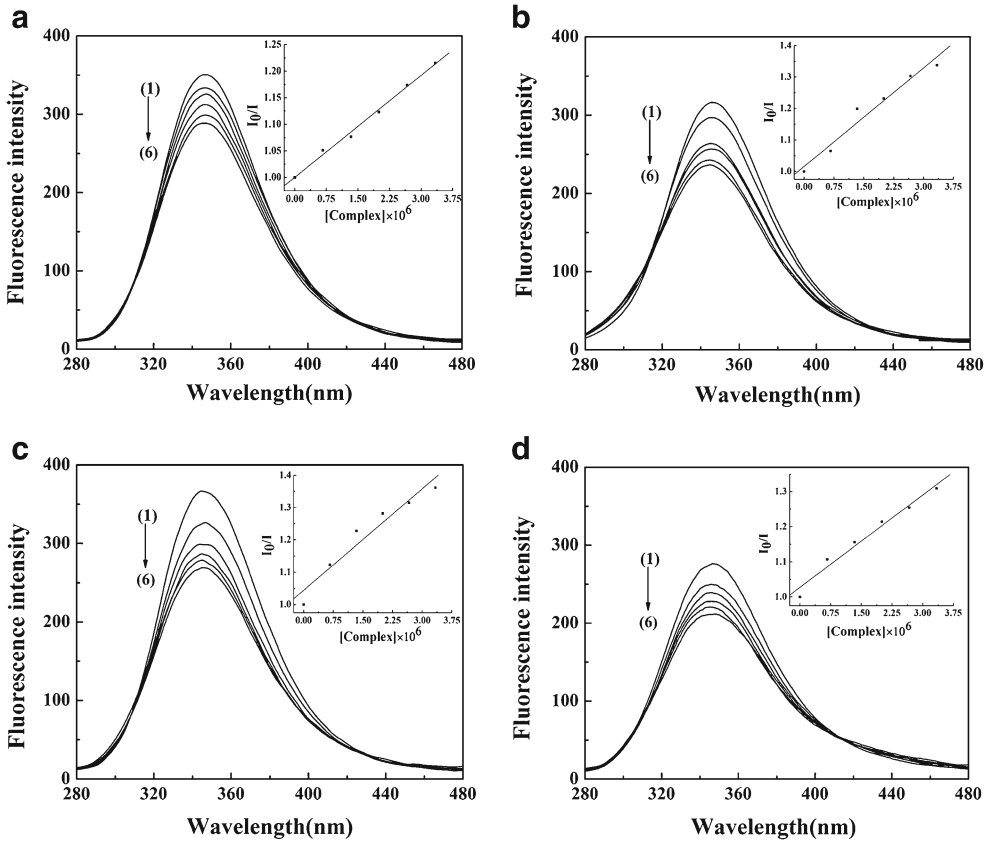

Fig. 6 Fluorescence spectra of BSA in the absence and the presence of complex. Inset: Stern-Volmer plots of the fluorescence titration data of the complexes. [BSA]=0.50×10^{-6} mol·L^{-1}; [compound]×10^8=0, 0.67, 1.33, 2.00, 2.67 and 3.33 mol·L^{-1}, from (1) to (6), respectively. λ_{ex}=255 nm. **a** complex **1**; **b** complex **2**; **c** complex **3**; **d** NCTD

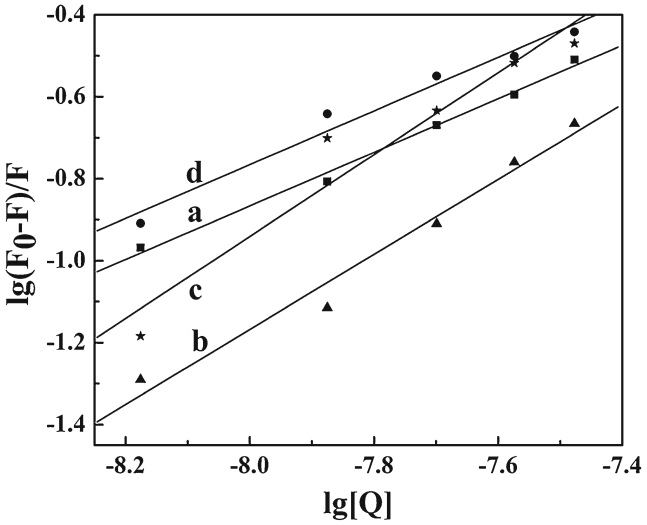

Fig. 7 Logarithmic plots of fluorescence quenching of BSA. a: NCTD, b: complex **1**, c: complex **2**, d: complex **3**

10^4 (**3**). The values of n were 0.66 (NCTD), 0.92 (**1**), 1.00 (**2**) and 0.67 (**3**). The results suggested that strong binding force existed between the complexes and BSA with complexes intensity stronger than NCTD.

According to the binding constants K_A, the order of the interaction intensity is **2**>**1**>**3**>NCTD, which is related with the different metal ions of the complexes. The results may be due to the hydrogen bonds or covalency interaction between complexes and amino-, carboxyl-, acyl- in BSA.

Effect of the Complexes on the BSA Conformation

The conformational changes in BSA were evaluated by the synchronous fluorescence intensity of protein amino acid residues. In the experiment, synchronous fluorescence spectra were used at different scanning intervals $\Delta\lambda$ ($\Delta\lambda=\lambda_{em}-\lambda_{ex}$). At $\Delta\lambda$=15 nm, the spectrum characteristic of tyrosine residues was observed, and at $\Delta\lambda$=60 nm, the spectrum characteristic of tryptophan residues was observed [33]. The results are shown in Fig. 8(a (**1**), b (**2**), c (**3**)) ($\Delta\lambda$= 60 nm). Results showed that fluorescence intensities of tyrosine were unchanged, while the fluorescence intensity changes of tryptophan were significant. A significant red-shift of tryptophan fluorescence upon the addition of the complexes is observed. These shifts result from the changes in the polarity around the tryptophan residues of BSA [34]. The hypochromism ratios of complexes to tryptophan residues (15.57 % (**1**), 24.17 % (**2**) and 26.21 % (**3**)) indicate that the main contribution is tryptophan residues [35].

Antiproliferative Activity Evaluation

The antiproliferative activities of the Na_2(DCA) and complexes **1**–**3** against human hepatoma cells (SMMC-7721)

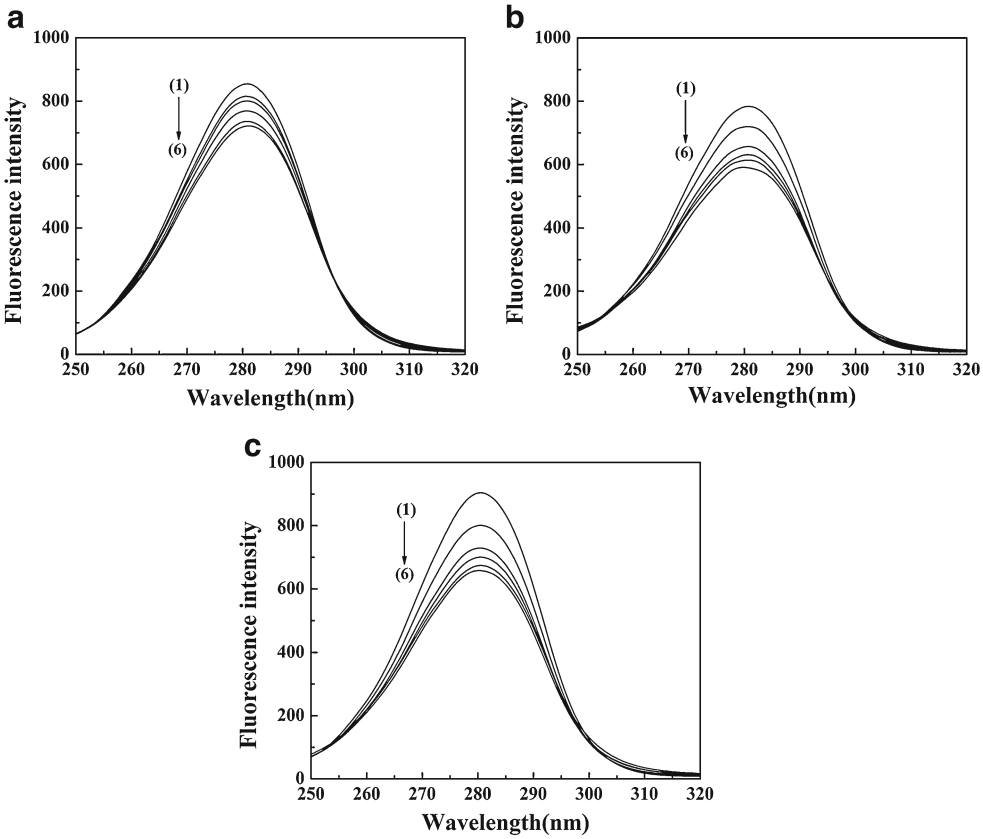

Fig. 8 Synchronous fluorescence spectra of BSA in the absence and the presence of complex ($\Delta\lambda$=60 nm). [BSA]= 0.5×10^{-6} mol·L^{-1}; [complex]× 10^8=0, 0.67, 1.33, 2.00, 2.67 and 3.33 mol·L^{-1}, from (1) to (6), respectively. a: complex **1**; b: complex **2**; c: complex **3**

(Fig. 9) and human gastric cancer cells (MGC80-3) (Fig. 10) were investigated in vitro. The values of IC_{50} for these compounds are listed in Table 5. The results showed complexes **1**–**3** had strong antiproliferative effect against two types of cancer cells in the tested concentration range. The inhibition effects were enhanced by increasing the concentration of complexes.

As shown in Fig. 9, the inhibition rates of complexes were significantly higher than $Na_2(DCA)$ ($P<0.01$) against human hepatoma cells. Especially at concentration of 75.00 μmol·L^{-1}, the inhibition intensities of complexes (67.8±3.2 (**1**), 69.9±4.6 (**2**), 81.2±1.2 (**3**)) were much stronger than $Na_2(DCA)$ (19.1±8.3). At the concentration lower than 150.00 μmol·L^{-1}, complexes **1** and **2** exhibited similar efficiency. Complex **3** was the most active species. The values of IC_{50} of complex **3** (43.52±2.82 μmol·L^{-1}) and NCTD (115.5±9.5 μmol·L^{-1}) [9] inferred that complex **3** had the strongest activities against human hepatoma cells. The result is consistent with complex **3** possesses the strongest interaction with DNA. So, we assume that the main target point of antiproliferative effect is DNA molecule for the complexes. The stability of DNA is strengthened after the complexes interacting with DNA with reducing susceptibility of DNA to enzyme. So, the function of DNA is hindered, which leads to the inhibition of cancer cells proliferative [36]. Meanwhile, because of the lipophilic 2-aminopyridine and hydrophilic [M$(DCA)_2$] ion, the complexes could easily channel through cancer cell membranes, and affect target molecule.

As shown in Fig. 10, the inhibition rates of complexes **1**–**3** were higher than the rate of $Na_2(DCA)$ ($P<0.01$) against human gastric cancer cells at the concentration of 75.00 μmol·L^{-1}. At other tested concentrations, the inhibition rates of complexes were very close to $Na_2(DCA)$. The values of IC_{50} of complex **2**

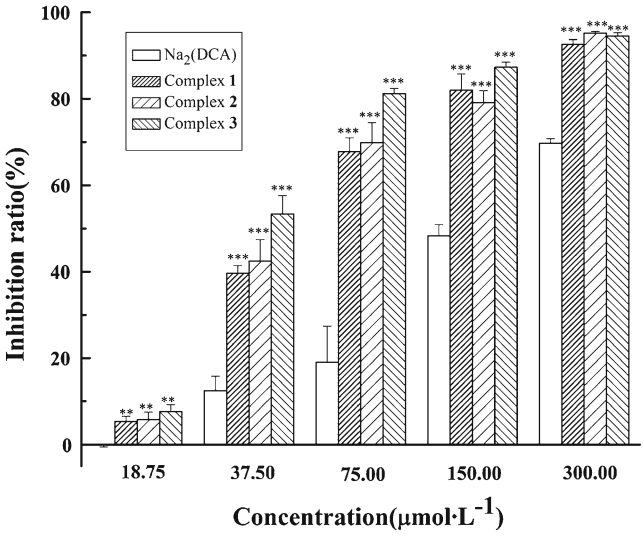

Fig. 9 Inhibition effects of complexes 1–3 and $Na_2(DCA)$ on SMMC-7721 cell growth. Data represent mean + S.D. and all assays were performed in triplicate for three independent experiments. *$P<0.05$, **$P<0.01$, ***$P<0.001$ vs $Na_2(DCA)$ in the same concentration, *t-test*

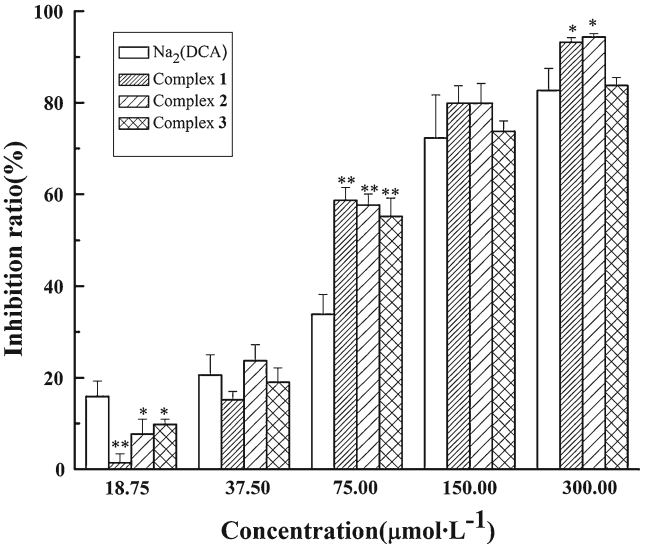

Fig. 10 Inhibition effects of complexes 1–3 and $Na_2(DCA)$ on MGC80-3 cell growth. Data represent mean + S.D. and all assays were performed in triplicate for three independent experiments. *$P<0.05$, **$P<0.01$, ***$P<0.001$ vs $Na_2(DCA)$ in the same concentration, *t-test*

(66.76±4.68 μmol·L^{-1}) indicated that complex **2** had more activity against human gastric cancer cells than others. And the order of the intensities is consistent with the order of binding constants of the interaction between complexes and BSA. So, the antiproliferative activities of complexes against human gastric cancer cells are possible due to the interaction of complexes with protein in the cancer cells.

Conclusions

Three novel transition metal complexes were synthesized. The chemical formula of the complexes are $(Hapy)_2$[M$(DCA)_2$]·$6H_2O$ (M=Mn (**1**), Ni (**2**) and Cu (**3**)). The structures of the complexes were determined by X-ray diffraction. The complexes crystallized in the triclinic crystal system with $P\bar{1}$ space group.

All the tested results suggest that the complexes could bind DNA, and the modes of the interaction are partial intercalation. Complex **3** gives the most intensive DNA binding. Meanwhile, the complexes could quench the fluorescence of BSA through static quenching. And complex **2**

Table 5 IC_{50} values (72 h) of complexes and $Na_2(DCA)$ on SMMC-7721 and MGC80-3 cells

IC_{50}(μmol·L^{-1})	SMMC-7721	MGC80-3
$Na_2(DCA)$	152.8±15.6	93.2±13.5
1	55.99±1.63	72.18±2.77
2	54.27±5.03	66.76±4.68
3	43.52±2.82	76.93±6.57

has the greatest quenching intensity. Tryptophan fluorescence spectra show a significant red-shift.

The antiproliferative activities testing reveal that all the complexes show strong inhibition ratios against human hepatoma cells and moderate inhibition ratios against human gastric cancer cells in vitro. For complex **3**, its inhibition ratio against human hepatoma cells was significantly stronger than NCTD, which has been widely used clinically. The complex of demethylcantharate copper(II) and 2-aminopyridine acid may be useful for designing new and more efficient anticancer drugs targeted to DNA.

The complexes possess the advantages of the good hydrophilcity as well as lipophilic, easy channeling through cell membranes etc. It also has low toxicity. These unique properties make ionic crystal a good compound for developing anti-cancer drugs.

Acknowledgements Financial support from Natural Science Foundation of Zhejiang Province, China (Grant No. Y407301) is gratefully acknowledged.

References

1. Adam MC, Michael CB, Elizabeth C, Alistair TRS, Jennette AS, Monique LB (2000) Anhydride modified Cantharidin analogues: synthesis, inhibition of Protein Posphatases 1 and 2A and anticancer activity. Bioorg Med Chem Lett 10:1687–1690
2. Wang CC, Wu CH, Hsieh KJ, Yen KY, Yang LL (2000) Cytotoxic effects of cantharidin on the growth of normal and carcinoma cell. Toxicology 147:77–87
3. Yin FL, Zou JJ, Xu L, Wang X, Li RC (2005) Synthesis, characterization and antitumor activity of Lanthanum(III) complex with Demethylcantharidate. J Rare Earths 23:596–599
4. Wang GS (1989) Medical use of mylabris in ancient china and recent studies. J Ethnopharmacol 26:147–162
5. Albert E, Gerhard Z, Esteban PV (1997) 7-oxa[2.2.1]bicycloheptane-2,3-dicarboxy-lic acid derivatives as phosphatase inhibitors. Bioorg Med Chem Lett 7:2513–2518
6. Wang YY, Hu RD, Lin QY, Zhao YL, Wang N (2010) Synthesis, crystal structure and antiproliferative activities of Mn(II) complexes of Demethylcantharate. Asian J Chem 22:5993–5999
7. Li SK, Lin QY, Lv TX, Wang YJ, Chen D (2010) Synthesis, crystal structure and DNA binding studies of a Nickel(II) complex with 2-Aminomethylbenzimidazole and Demethylcantharate. Chinese J Struct Chem 29:1632–1637
8. Zhang F, Zhu WZ, Lin QY, Guo WD, Zhang LL, Li SK (2011) Synthesis, characterization and DNA binding of the complexes of rare earth with phenanthroline and demethylcantharate. J Rare Earths 29:297–302
9. Wang N, Lin QY, Feng J, Zhao YL, Wang YJ, Li SK (2010) Crystal structures, DNA interaction and antiproliferative activities of the cobalt(II) and zinc(II) complexes of 2-amino-1,2,3-thiadiazole with demethylcantharate. Inorg Chim Acta 363:3399–3406
10. Wang N, Lin QY, Wen YH, Kong LC, Li SK, Zhang F (2012) Crystal structures, DNA interaction and growth inhibitory activities of the cobalt(II) and nickel(II) complexes of 2-aminothiazole with demethylcantharate. Inorg Chim Acta 384:345–351
11. Lin QY, Wang YY, Feng YL, Yan DM, Wang YJ, Zhang F (2011) Crystal structure, DNA interaction, and antiproliferative activities of the cobalt(II) complex of demethylcantharate and imidazole. J Coord Chem 64:920–930
12. Abu-Youssef MAM, Soliman SM, Langer V, Gohar YM, Hasanen AA, Makhyoun MA, Zaky AH, Öhrström LR (2010) Synthesis, crystal structure, quantum chemical calculations, DNA interactions, and antimicrobial activity of $[Ag(2\text{-amino-3-methylpyridine})_2]NO_3$ and $[Ag(\text{pyridine-2-carboxaldoxime})NO_3]$. Inorg Chem 49:9788–9797
13. Bhat SS, Kumbhar AS, Lönnecke P, Hey-Hawkins E (2010) Self-Association of Ruthenium(II) Polypyridyl complexes and their interactions with Calf Thymus DNA. Inorg Chem 49:4843–4853
14. To KKW, Ho YP, Au-Yeung SCF (2002) Determination of the release of hydrolyzed demethylcantharidin from novel traditional Chinese medicine-platinum compounds with anticancer activity by gas chromatography. J Chromatogr A 947:319–326
15. Geary WJ (1971) The use of conductivity measurements in organic solvents for the characterization of coordination compounds. Coord Chem Rev 7:81–122
16. Nagababu P, Satyanarayana S (2007) DNA binding and cleavage properties of certain ethylenediamine cobalt(III) complexes of modified 1,10-phenanthrolines. Polyhedron 26:1686–1692
17. Zheng XL, Sun HX, Liu XL, Chen YX, Qian BC (2004) Astilbic acid induced COLO 205 cell apoptosis by regulating Bcl-2 and Bax expression and activating caspase-3. Acta Pharmacol Sin 25:1090–1095
18. Sheldrick GM (1997) SHELXS 97. Program for the Solution of Crystal Structures. University of Gottingen, Germany
19. Sheldrick GM (1997) SHELXL 97. Program for the Refinement of Crystal Structures. University of Gottingen, Germany
20. Zhang F, Zhang QQ, Wang WG, Wang XL (2006) Synthesis and DNA binding studies by spectroscopic and PARAFAC methods of a ternary copper(II) complex. J Photoch Photobio A 184:241–249
21. Sethu R, Dhanasekaran S, Eringathodi S, Vaiyapuri SP, Mohammad AA, Mallayan P (2011) Ternary Dinuclear Copper(II) complexes of a Hydroxybenzamide ligand with Diimine Coligands: the 5,6-dmp ligand enhances DNA binding and cleavage and induces apoptosis. Inorg Chem 50:6458–6471
22. Chen GJ, Qiao X, Qiao PQ, Xu GJ, Xu JY, Tian JL, Gu W, Liu X, Yan SP (2011) Synthesis, DNA binding, photo-induced DNA cleavage, cytotoxicity and apoptosis studies of copper(II) complexes. J Inorg Biochem 105:119–126
23. Wu SS, Yuan WB, Wang HY, Zhang Q, Liu M, Yu KB (2008) Synthesis, crystal structure and interaction with DNA and HAS of (N, N′-dibenzylethane-1,2-diamine) transition metal complexes. J Inorg Biochem 102:2026–2034
24. Gao EJ, Zhu MM, Liu L, Huang Y, Wang L, Shi CY, Zhang WZ, Sun YG (2010) Impact of the carbon chain length of novel Palladium(II) complexes on interaction with DNA and cytotoxic activity. Inorg Chem 49:3261–3270
25. Zhu WZ, Lin QY, Lu M, Hu RD, Zheng XL, Cheng JP, Wang YY (2009) Synthesis, characterization, DNA-Binding and antiproliferative activity of Nd(III) complexes With N-(Nitrogen Heterocyclic) Norcantharidin Acylamide Acid. J Fluoresc 19:857–866
26. Satyanarayana S, Dabrowiak JC, Chaires JB (1993) Tris(phenanthroline) ruthenium(II) Enantiomer Interactions with DNA: mode and specificity of binding. J Biochem 32:2573–2584
27. Wang K, Zhang Z, Guo QN, Bao XP, Li ZY (2007) Studies on interaction of water-soluble bridged Porphyrin with DNA. Acta Chim Sinica 22:2597–2603
28. Ashoka S, Seetharamappa J, Kandagal PB, Shaikh SMT (2006) Investigation of the interaction between trazodone hydrochloride and bovine serum albumin. J Lumin 121:179–186
29. Wang YJ, Hu RD, Jiang DH, Zhang PH, Lin QY, Wang YY (2011) Synthesis, crystal structure, interaction with BSA and antibacterial activity of La(III) and Sm(III) complexes with Enrofloxacin. J Fluoresc 21:813–823

30. Tang RR, Tang CH, Tang CQ (2011) Synthesis, luminescence properties of a novel aromatic carboxylic acid (L) and corresponding Eu(III) and Tb(III) compounds as well as the binding characteristics of L with bovine serum albumin (BSA). J Organomet Chem 696: 2040–2046
31. Filitsa D, Franc P, Vassilis T, Iztok T, Dimitris PK, George P (2011) Interaction of copper(II) with the non-steroidal anti-inflammatory drugs naproxen and diclofenac: Synthesis, structure, DNA- and albumin-binding. J Inorg Biochem 105:476–489
32. Mariam J, Dongre PM, Kothari DC (2011) Study of Interaction of Silver Nanoparticles with Bovine Serum Albumin Using Fluorescence Spectroscopy. J Fluoresc. doi:10.1007/s10895-011-0922-3
33. Wang CX, Yan FF, Zhang YX, Ye L (2007) Spectroscopic investigation of the interaction between rifabutin and bovine serum albumin. J Photoch Photobio A 192:23–28
34. Hu YJ, Liu Y, Zhao RM, Dong JX, Qu SS (2006) Spectroscopic studies on the interaction between methylene blue and bovine serum albumin. J Photoch Photobio A 179:324–329
35. Liu B, Guo Y, Wang J, Xu R, Wang X, Wang D, Zhang LQ, Xu YN (2010) Spectroscopic studies on the interaction and sonodynamic damage of neutral red (NR) to bovine serum albumin (BSA). J Lumin 130:1036–1043
36. Zhang JM, Li RF, Liu SX (1999) A relation between stability of transition metal shiff base complexes and their disinfectivity. Chinese J Inorg Chem 15:493–496